J Mater Sci (2008) 43:2785–2791
DOI 10.1007/s10853-008-2516-2

Oxidation behavior of Cr_2AlC ceramics at 1,100 and 1,250 °C

Wubian Tian · Peiling Wang · Yanmei Kan · Guojun Zhang

Received: 28 November 2007 / Accepted: 29 January 2008 / Published online: 28 February 2008
© Springer Science+Business Media, LLC 2008

Abstract The isothermal oxidation behavior of Cr_2AlC ceramics oxidized in air at 1,100 and 1,250 °C for 20 h was studied. The phase compositions and microstructure of the oxidized surface were identified and observed by XRD and electron probe microanalysis (EMPA), respectively, while the cross sections of oxidized samples were also examined by EMPA equipped with energy dispersive spectrum capabilities. The results indicated that the oxidation of Cr_2AlC samples was carried out by the outward diffusion of Al, together with small amounts of Cr, and the inward diffusion of O to form a surface layer of α-Al_2O_3, while carbides (Cr_7C_3 and Cr_3C_2), rather than oxides (Cr_2O_3), were formed in a layer under the surface. The mass gain per unit surface area of oxidized Cr_2AlC followed a parabolic relation with oxidation time, and the parabolic rates, k_p, for oxidation at 1,100 and 1,250 °C were 1.1×10^{-12} and 7.1×10^{-10} kg^2 m^4 s^{-1}, respectively.

Introduction

Cr_2AlC belongs to a large class of solids with the general formula $M_{n+1}AX_n$ (abbreviated as MAX, where $n = 1, 2, 3$, M is an early transition metal, A is an A-group (mostly IIIA or IVA) element, and X is C or N). In this family of compounds, Ti_3SiC_2 is the material that has been extensively studied since great progress in synthesis was made by Barsoum's group in 1996 [1]. The results show that Ti_3SiC_2 possesses unique combined properties of both metals and ceramics as it is lightweight and easily machinable, exhibits high elastic modulus, good thermal shock resistance, and damage tolerance. For M_2AX phases, systematic study has been scarce, and previous work mainly focused on synthesis and characterization of Ti_2AlC, Nb_2AlC, and their solid solutions [2, 3]. In recent years, there were several papers to report the results of theoretical calculations dealing with M_2AX compounds [4–6]. Research into the synthesis and properties of bulk Cr_2AlC material has also been carried out [7–11]. The results indicate that Cr_2AlC exhibits excellent metallic and ceramic properties. Like Ti_3SiC_2 and Ti_2AlC, Cr_2AlC is relatively soft (Vickers hardness of 5.2 [9]–5.5 [7]), elastically stiff (Young's modulus of 288 GPa, shear modulus of 116 GPa [8, 9]) with flexural strength and compressive strength being 483 and 1159 MPa [9], respectively, electrically and thermally conductive, and readily machinable [8].

Up to now, there have been few papers related to the investigation of high temperature oxidation of bulk Cr_2AlC ceramics. Lin et al. [7] performed a brief oxidation study at 1,200 °C in air and reported its excellent oxidation resistance. The same authors also researched high-temperature oxidation and hot corrosion of Cr_2AlC at 800–1,300 °C in air [12]. Lee et al. [13] studied oxidation behavior of Cr_2AlC at 1,300 °C. The samples of bulk Cr_2AlC in the latter two studies were prepared by hot-pressing using chromium and/or chromic carbides, as well as aluminum, as starting materials [12, 13].

In the present work, Cr_2AlC ceramics were fabricated by hot pressing of a mixture of chromium, aluminum, and graphite powders at 1,400 °C for 1 h [9]. The isothermal oxidation behavior of Cr_2AlC samples was studied by means of X-ray diffraction (XRD) and electron probe

W. Tian · P. Wang (✉) · Y. Kan · G. Zhang
State Key of High Performance Ceramics and Superfine Microstructure, Shanghai Institute of Ceramics, Chinese Academy of Sciences, Shanghai 200050, China
e-mail: plwang@sunm.shcnc.ac.cn

microanalysis (EPMA) equipped with energy dispersive spectrum (EDS) capabilities, through which the phase compositions of the oxidized surface were identified, microstructures of surfaces and cross sections of the oxidized samples were observed, and the elemental distribution in cross section was analyzed. Finally, the oxidation kinetics of Cr_2AlC ceramics was discussed.

Experimental procedures

Chromium (200 mesh, purity of 99.95%, Shanghai Chemical Reagent Company of National Medicine Group, China), milled for 8 h using Si_3N_4 ball (3 and 10 mm in diameter with weight ratio to be 2:1, Huasheng Fine Ceramics Co. Ltd., Jintan, Jiangsu Province, China) as milling media in a planetary ball mill to produce an average particle size of 3 μm, together with aluminum ($D_{50} = 3$ μm, purity of 99%, Shanghai Chemical Reagent Company of National Medicine Group) and graphite powders (3200 mesh, purity of 99%, Shanghai Colloid Chemical Plant) were used as raw materials. The powders were weighed according to the molar composition Cr:Al:C = 2:1.1:1 and milled in absolute alcohol for 24 h, using Si_3N_4 ball (3 mm in diameter, Huasheng Fine Ceramics Co. Ltd., Jintan, Jiangsu Province, China) as milling media. Powder compacts were hot-pressed (30 MPa) at 1,400 °C for 1 h in flowing Ar with a heating rate of 35 °C/min.

Densities of the sintered samples were measured by Archimedes principle. Phase compositions were determined by XRD (D/max 2550 V, Japan). Microstructural observation of oxidized surfaces was performed by means of an electron probe microanalyzer (JEOL JXA-8100F, Japan) equipped with EDS, while the backscattered electron (BSE) image was used for microstructural observation of polished cross sections of the oxidized samples.

The isothermal oxidation of Cr_2AlC samples was carried out in a simultaneous thermal analyzer (STA 409PC Luxx, Germany). The surfaces of samples with a dimension of $3 \times 5 \times 8$ mm^3 were ground down to 3000 grit SiC sand and polished to 1 μm by diamond paste before the oxidation. Samples were heated in air to 1,100 and 1,250 °C for 20 h at a heating rate of 20 °C/min, with the weight gains recorded continuously as a function of time.

Results

Phases of the oxide scale

A XRD pattern of bulk Cr_2AlC sample hot-pressed at 1,400 °C for 1 h is shown in Fig. 1a, while the XRD patterns of Cr_2AlC samples oxidized at 1,100 and 1,250 °C for 20 h are shown in Fig. 1b and c, respectively.

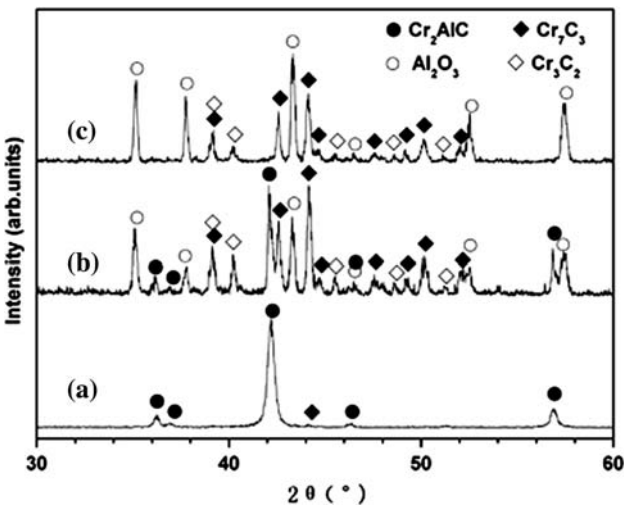

Fig. 1 XRD patterns of (**a**) as-sintered bulk Cr_2AlC sample, (**b**) Cr_2AlC sample oxidized at 1,100 °C in air for 20 h, and (**c**) Cr_2AlC sample oxidized at 1,250 °C in air for 20 h

It was found that hot-pressed sample consisted of Cr_2AlC, as an almost single phase, together with trace amount of Cr_7C_3. Four phases were detected in the Cr_2AlC sample oxidized at 1,100 °C, i.e., Cr_2AlC, Cr_7C_3, Cr_3C_2, and α-Al_2O_3, in which the amounts of Cr_2AlC and Cr_7C_3 were comparable, followed by lesser amounts of α-Al_2O_3 and Cr_3C_2. Since the scale of the sample oxidized at 1,100 °C was thin, noticeably thinner than 10 μm, as shown in Fig. 4a, it was believed that the appearance of Cr_2AlC phase in Fig. 1b was attributed to the bulk matrix under the oxidation layer, as discussed in "Morphology and phase analysis of cross section" and "Discussions" section.

The Cr_2AlC sample oxidized at 1,250 °C included three phases: α-Al_2O_3, Cr_7C_3, and Cr_3C_2, in which α-Al_2O_3 became the main phase, while Cr_7C_3 and Cr_3C_2 contents decreased in comparison to the samples oxidized at 1,100 °C.

It was noted that the occurrence of the strongest XRD peak of the Al_2O_3 phase at a 2θ value of around 43.3° in the oxidized samples fitted better with a Cr-containing Al_2O_3 phase, $Al_{1.98}Cr_{0.02}O_3$ (JCPDS card No. 88-0883) when oxidation temperature was increased from 1,100 to 1,250 °C. The result will be further analyzed by EDS (see section "Morphology and phase analysis of cross section").

Oxidation kinetics of Cr_2AlC samples

The functions of mass gain of per unit surface area with oxidation time for the Cr_2AlC samples oxidized in air at 1,100 and 1,250 °C are shown in Fig. 2a, in which the

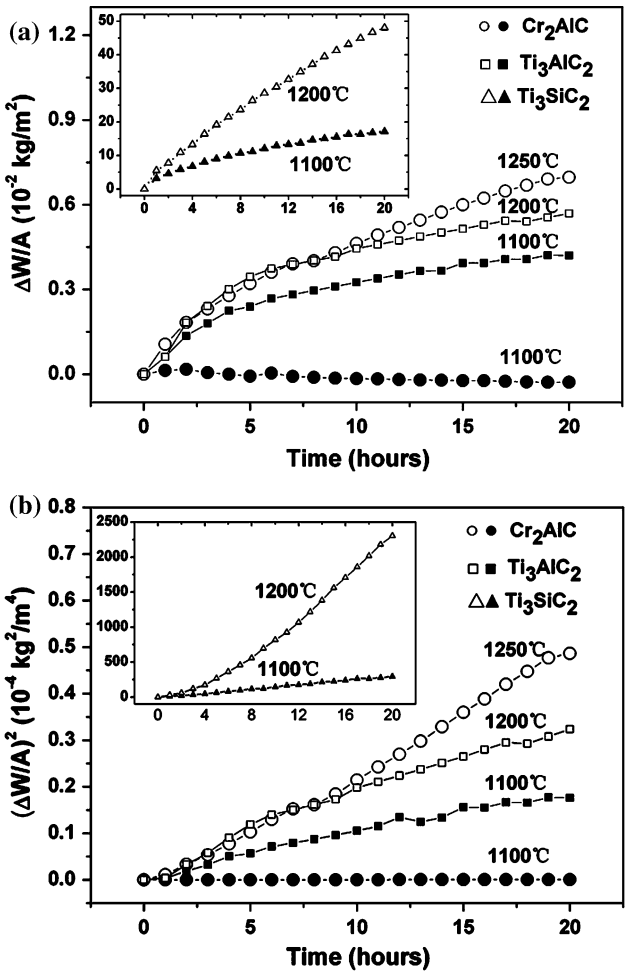

Fig. 2 (**a**) Mass gain per unit surface area versus oxidation time and (**b**) square of mass gain per unit surface area as a function of oxidation time for Cr_2AlC sample oxidized at 1,100 and 1,250 °C in air. The mass gain curves of Ti_3AlC_2 and Ti_3SiC_2 are also illustrated for comparison

mass gain curves of Ti_3SiC_2 and Ti_3AlC_2 are also illustrated for comparison [14, 15]. It was found that the mass gain of Cr_2AlC kept almost constant with the extension of oxidation time at 1,100 °C, and that they were not only smaller than that of Ti_3AlC_2 but were also two orders of magnitude smaller than that of Ti_3SiC_2. When the oxidation temperature was increased to 1,250 °C, the mass gain of Cr_2AlC was smaller than that of Ti_3AlC_2 oxidized at 1,200 °C for the first 7 h of the oxidation process and slightly higher beyond that. The mass gain of Cr_2AlC oxidized at 1,250 °C was clearly still much smaller than that of Ti_3SiC_2 oxidized at 1,200 °C.

Figure 2b presents the square of mass gain per unit surface area of Cr_2AlC sample as a function of oxidation time, in which the square of mass gain curves of Ti_3AlC_2 and Ti_3SiC_2 are also plotted for comparison. It was found that the square of mass gain per unit surface area had a linear function with oxidation time for Cr_2AlC sample, implying that mass gain of per unit surface area followed a parabolic relation with oxidation time. Thus the mass gain curves could be described by Eq. 1 as follows:

$$(\Delta W/A)^2 = k_p \cdot t \tag{1}$$

where $\Delta W/A$ is the mass gain per unit surface area, k_p is the parabolic rate constant, and t is oxidation time. It was obtained that the parabolic rates, k_p, of the Cr_2AlC samples oxidized at 1,100 and 1,250 °C were 1.1×10^{-12} and 7.1×10^{-10} $kg^2\ m^{-4}\ s^{-1}$, respectively, based on the results of Fig. 2b. It was noted that the k_p value of the Cr_2AlC sample oxidized at 1,250 °C for 20 h fits well with that of a Cr_2AlC sample oxidized at 1,200 °C for 50 h (6.8×10^{-10} $kg^2\ m^{-4}\ s^{-1}$) [7]. Table 1 lists the parabolic rate constants of Cr_2AlC, Ti_3SiC_2, and Ti_3AlC_2, in which the k_p of Cr_2AlC at 1,250 °C can be seen to be the same magnitude as Ti_3AlC_2 at 1,200 °C [15], while k_p of Cr_2AlC at 1,100 °C is two orders of magnitude smaller than that of Ti_3AlC_2 under the same temperature. As compared to Ti_3SiC_2, the parabolic rate constant of the Cr_2AlC sample at 1,250 °C is three orders magnitude smaller than that of Ti_3SiC_2 at 1,200 °C [14].

Morphology observation on the scales of Cr_2AlC samples

Surface morphology

The SEM micrographs of surfaces from the Cr_2AlC samples oxidized at 1,100 and 1,250 °C for 20 h are shown in Fig. 3a and b, respectively. The lamellar morphology of oxidized products was found on the surface of the sample oxidized at 1,100 °C. After the increase in oxidation temperature to 1,250 °C, the lamellar-like products thickened, piled up, and became linked with each other as shown in Fig. 3c.

Table 1 Parabolic rate constants, k_p, of Cr_2AlC, Ti_3SiC_2, and Ti_3AlC_2 phases

MAX phase	Oxidation temperature (°C)	Parabolic rate constants k_p ($kg^2\ m^{-4}\ s^{-1}$)	References
Cr_2AlC	1,100	1.1×10^{-12}	This work
	1,250	7.1×10^{-10}	This work
	1,200	6.8×10^{-10}	[7]
Ti_3SiC_2	1,200	6.58×10^{-7}	[14]
Ti_3AlC_2	1,100	2.7×10^{-10}	[15]
	1,200	4.2×10^{-10}	[15]

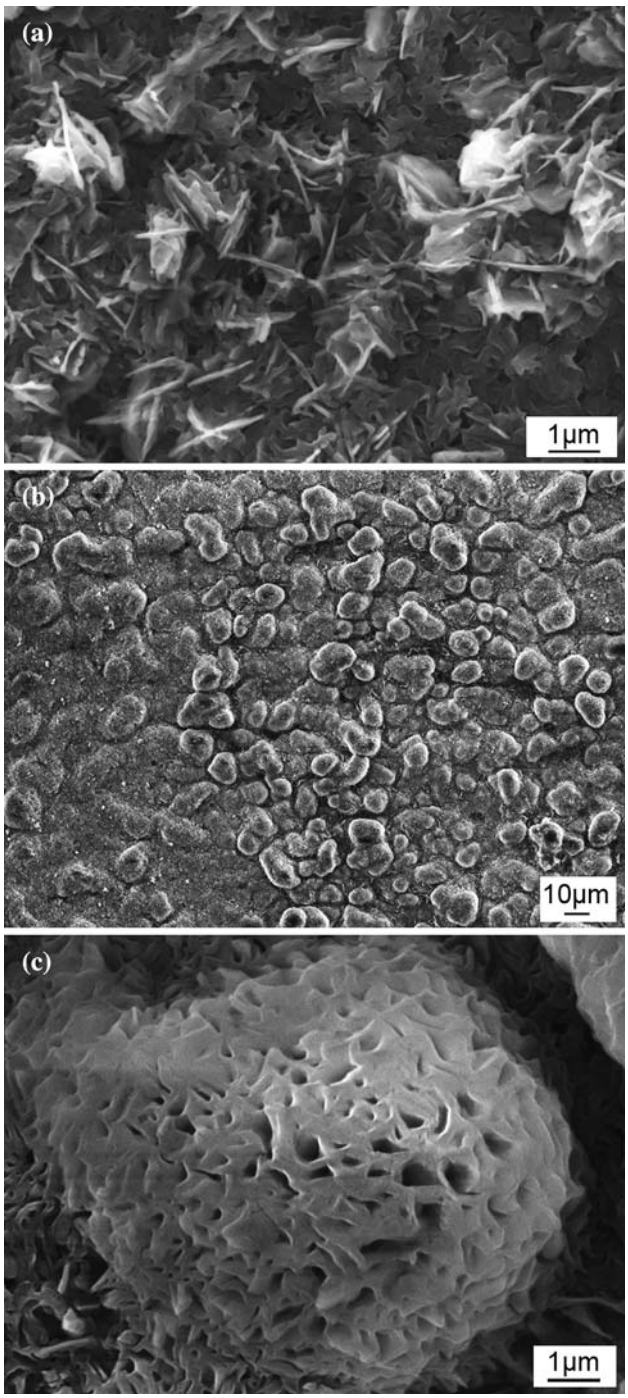

Fig. 3 Typical surface morphologies of the Cr_2AlC samples oxidized at (**a**) 1,100 °C and (**b**) 1,250 °C for 20 h. (**c**) The magnified image of one cocoon-like particle in (**b**)

Morphology and phase analysis of cross section

A SEM micrograph of the cross section of the Cr_2AlC sample oxidized at 1,100 °C for 20 h using BSE imaging is shown in Fig. 4a. It could be easily seen that the scale consisted of two layers, marked 1 and 2, while area 3 was the matrix. The brightness of the three areas had the order of area 2 > area 3 > area 1, revealing that the average atomic weight of the areas followed area 2 > area 3 > area 1.

The EDS patterns of area 1–3 are shown in Fig. 4b to d, respectively. It could be concluded based on EDS patterns combined with the XRD results that the outer dark and continuous layer was Al_2O_3 (marked 1) with an average thickness of ~2 μm, the white layer was formed by a mixed phase of Cr_7C_3 and Cr_3C_2 (marked 2) with a thickness of ~4 μm, and the light gray layer corresponded to the Cr_2AlC matrix (marked 3). It was noted that there were some weak peaks of Cr appearing in Fig. 4b, revealing the existence of trace amount of Cr in Al_2O_3 that agreed well with XRD results. A minor amount of chromium detected in the outmost Al_2O_3 oxide scale by EDS has also been reported in other literatures [12].

Figure 5a is a cross-sectional SEM BSE image of the Cr_2AlC sample oxidized at 1,250 °C for 20 h. The corresponding EDS patterns of areas 1–4 marked in Fig. 5a are shown in Fig. 5b–e, respectively. The scale of this Cr_2AlC sample, like the one oxidized at 1,100 °C, also consisted of two layers: the outer layer of Al_2O_3 phase (marked 1) with an average thickness of ~5 μm and a layer consisting of mixed Cr_7C_3 and Cr_3C_2 (marked 2) with an average thickness of ~10 μm. Area 3 was the Cr_2AlC matrix. It was noted that there were a few dark areas, other than voids, in the mixed layer containing Cr_7C_3 and Cr_3C_2 (see Fig. 5a), which more or less could also be found in Fig. 4a. The average atomic weight of the dark areas should be smaller than that of Cr_2AlC and equivalent with that of Al_2O_3, judging from the colors shown in area 4 of Fig. 5a. From a close look at Fig. 5d and e, it was found that the peaks appearing in both EDS patterns were similar, and the differences between them were the higher intensities in the Al peak and one Cr peak that overlapped O at about 0.55 keV shown in Fig. 5d, implying that the dark areas, like that labeled 4 in Fig. 5a, resulted from a mixture of unoxidized Cr_2AlC (not completely) and Al_2O_3. The results agreed with work on oxidation of Cr_2AlC at 1,300 °C in air [13], which reported the formation of an Al_2O_3 layer at the surface and an underlying Cr_7C_3 layer containing voids with some Al_2O_3 islands.

It is well known that there is a limitation with X-ray penetration, in that XRD patterns normally represent results from the sample with a depth of up to tens of microns below the surface. Therefore, it was understood that the matrix phase, Cr_2AlC, could be detected in the sample oxidized at 1,100 °C, as shown in Fig. 1b, since the total thickness of the two layers was ~6 μm. The matrix phase did not appear in the XRD pattern of the sample oxidized at 1,250 °C, as shown in Fig. 1c, implying that X-ray penetration was <20 μm as the oxidized scale of the sample was ~15 μm.

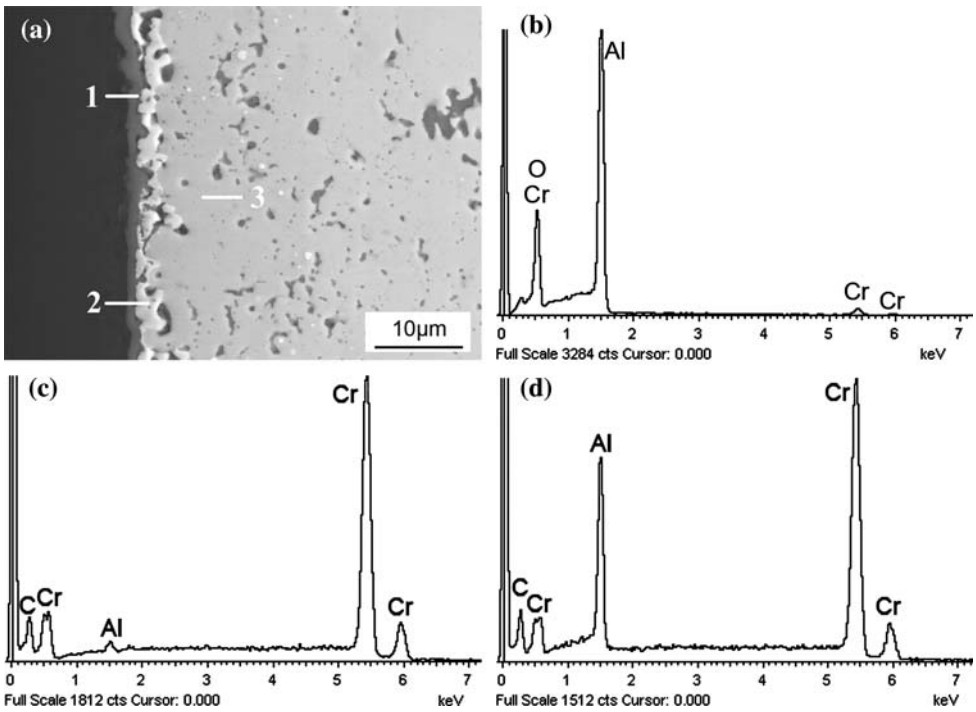

Fig. 4 (**a**) A BSE image of the cross section of Cr_2AlC sample oxidized at 1,100 °C for 20 h, (**b**)–(**d**) the corresponding EDS patterns of areas 1–3 marked in (**a**)

Discussions

It was reported that the scales formed on the surfaces of oxidized Ti_3SiC_2 [14, 16, 17] consisted of an outer layer of pure TiO_2 and an inner layer of mixed TiO_2 and SiO_2. For Ti_3AlC_2, the scales were mainly composed of an outer layer of TiO_2 and an inner layer of Al_2O_3 [15], while as oxidation continued, either alternating thick TiO_2/thin Al_2O_3 multilayers or $TiO_2/Al_2O_3/(TiO_2+Al_2O_3)$ triple layers were formed [18]. In the present case, on the basis of microstructural observation of the cross section and phase analysis of oxidized samples in the present case, it was found that the scales of Cr_2AlC oxidized in air consisted of an outer layer of Al_2O_3 with a small amount of dissolved Cr and an inner mixed layer of Cr–C, in which the Al_2O_3 content increased with an increase in oxidation temperature. It was easy to understand that outward diffusion of Al together with a small amount of Cr and inward diffusion of O to form Al_2O_3 on the surface layer during the oxidation process, while the appearance of chromium carbides, including Cr_7C_3 and Cr_3C_2, rather than Cr_2O_3 in the inner layer of oxidized samples, suggested that Cr in Cr_2AlC sample was mainly transferred to carbides.

From a thermodynamic point of view of the oxidation process, Gibbs energies of the formation of Al_2O_3 and Cr_2O_3 were −1582.3 kJ/mol [19] and −1058.1 kJ/mol [20], respectively, implying that the formation of Al_2O_3 was easier than that of Cr_2O_3. In other words, when Cr and Al coexisted and the kinetic conditions were satisfied, the formation of Al_2O_3 was preferred.

It should be noted that the single continuous and protective layer of Al_2O_3 has been the key point for the excellent oxidation resistance of Cr_2AlC, as compared with the multilayer of pure TiO_2 with TiO_2/SiO_2 formed during the oxidation of Ti_3SiC_2 [14]. It was noted that the oxidation resistance of Ti_3SiC_2 was significantly improved by the substitution of Si with 10 at.% of Al to obtain a $Ti_3Si_{0.9}Al_{0.1}C_2$ solid solution, in which a continuous Al_2O_3 layer was formed at the temperature range of 1,000–1,300 °C [21].

On the basis of the above results, it could be concluded that oxidation of the Cr_2AlC samples was carried out by outward diffusion of Al together with small amounts of Cr and inward diffusion of O to form a Cr-containing Al_2O_3 phase on the surface layer, while the remaining oxidation products, Cr_7C_3 and Cr_3C_2, were in the inner layer. Accordingly, the reactions for Cr_2AlC during oxidation could be described by the following formulas:

$$28Cr_2AlC + 23O_2 \rightarrow 14Al_2O_3 + 8Cr_7C_3 + 4CO \quad (2)$$

$$20Cr_2AlC + 15O_2 \rightarrow 10Al_2O_3 + 4Cr_7C_3 + 4Cr_3C_2 \quad (3)$$

With the increase of oxidation temperature, the amount of Al_2O_3 increased, i.e., the scale thickened. As the oxidation products, the volume of Cr_7C_3 and Cr_3C_2 would also increase, leading to the growth of the mixed Cr–C layer. The oxidation rate would be controlled by the interdiffusion of Al and O through this growing carbide layer.

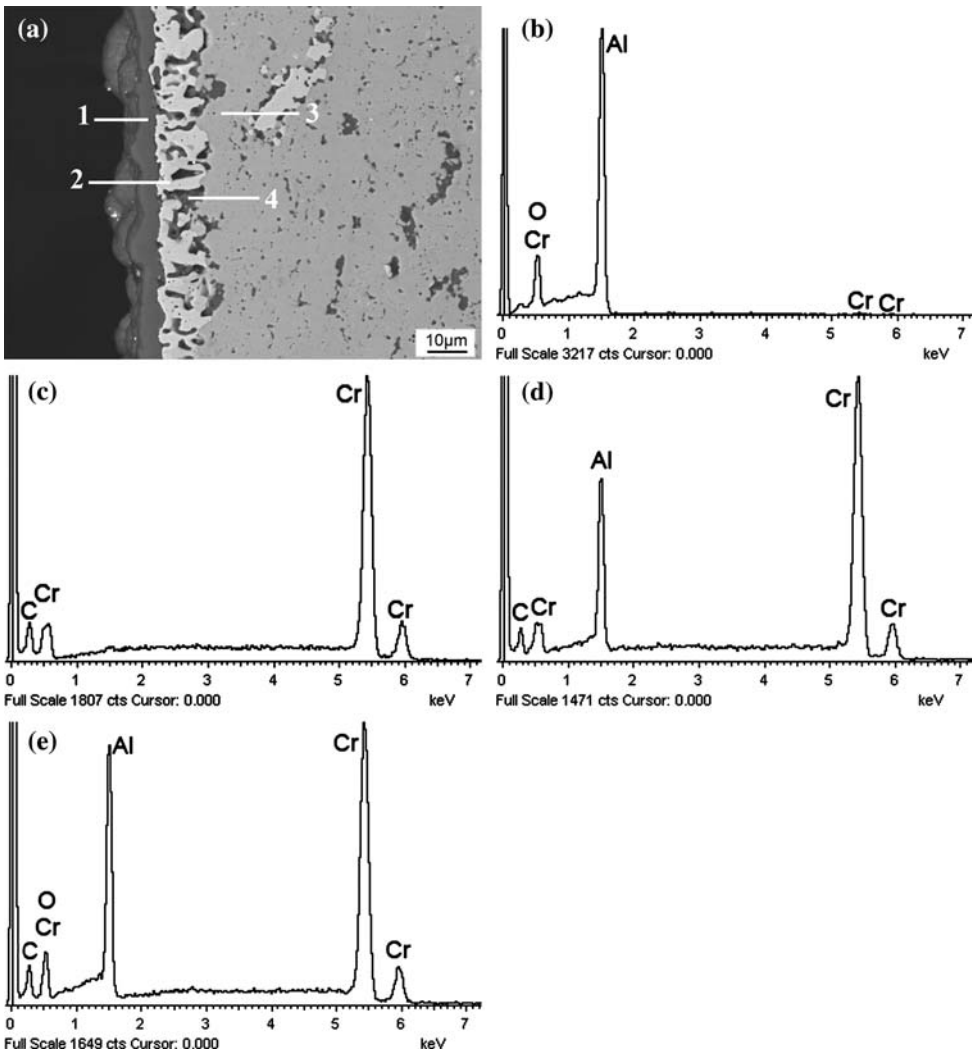

Fig. 5 (**a**) A BSE image of the cross section of Cr_2AlC sample oxidized at 1,250 °C for 20 h, (**b**)–(**e**) the corresponding EDS patterns of areas 1–4 marked in (**a**)

It was thought that the Cr_7C_3 and Cr_3C_2 phases did not further oxidize into Cr_2O_3 in the experimental conditions was resulted from the formation of Al_2O_3 layer that provided excellent protection against oxidation. Figure 6 is a scheme outlining qualitatively the evolution of the oxide scale of Cr_2AlC associated with limitation of X-ray penetration, thus to understand the occurrence of phases on the oxidized surface shown in Fig. 1. It is believed that the oxidized phase appearing in XRD pattern would consist of Al_2O_3 only by further increase in oxidation temperature or time.

Conclusions

The isothermal oxidation behavior of Cr_2AlC oxidized at 1,100 and 1,250 °C, which was synthesized by hot-pressing a mixture of chromium, aluminum, and graphite powders, was studied. The oxidation process for the Cr_2AlC samples was carried out by outward diffusion of Al together with small amounts of Cr and inward diffusion of O to form a Cr-containing Al_2O_3 phase on the surface layer, while the remaining oxidation products, Cr_7C_3 and Cr_3C_2, were formed in an inner layer under the surface. Thus the scale of Cr_2AlC samples consisted of two layers. One was an outer continuous and dense layer of Al_2O_3. The second inner layer between the Al_2O_3 top layer and the Cr_2AlC substrate consisted of chromium carbides (Cr_7C_3 and Cr_3C_2), in which some unoxidized Cr_2AlC and Al_2O_3 were included. The oxidation rate would be controlled by the inter-diffusion of Al and O through this growing carbide layer. The mass gain per unit surface area of oxidized Cr_2AlC followed a parabolic relation with oxidation time, and the parabolic rates, k_p, for oxidization at 1,100 and 1,250 °C were 1.1×10^{-12} and 7.1×10^{-10} $kg^2 \cdot m^4 \cdot s^{-1}$, respectively.

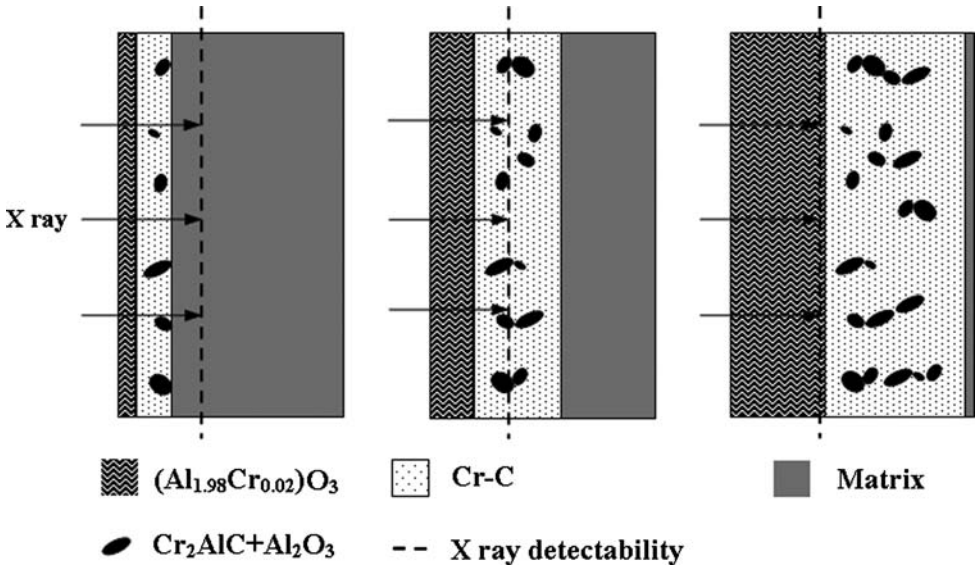

Fig. 6 Schematic depicting the evolution of the Cr_2AlC oxide scale

Acknowledgements This financial support from the Science and Technology Commission of Shanghai (Contract No. 04JC14076) was highly appreciated. The authors thank Prof. S.C. Zhang from University of Missouri—Rolla, USA, for technically reviewing this manuscript.

References

1. Barsoum MW, El-Raghy T (1996) J Am Ceram Soc 79:1953
2. Barsoum MW, Ali M, El-Raghy T (2000) Met Mater Trans 31A:1857
3. Barsoum MW, Golczewski J, Seifert HJ, Aldinger F (2002) J Alloy Compd 340:173
4. Sun ZM, Ahuja R, Li S, Schneider JM (2003) Appl Phys Lett 83:899
5. Sun ZM, Li S, Ahuja R, Schneider JM (2004) Solid State Commun 129:589
6. Lofland SE, Hettinger JD, Harrell K, Finkel P (2004) Appl Phys Lett 84:508
7. Lin ZJ, Zhou YC, Li MS, Wang JY (2005) Z Metallkd 96:291
8. Tian WB, Wang PL, Zhang GJ, Kan YM, Li YX, Yan DS (2006) Script Mater 54:841
9. Tian WB, Wang PL, Zhang GJ, Kan YM, Li YX (2007) J Am Ceram Soc 90:1663
10. Tian WB, Wang PL, Zhang GJ, Kan YM, Li YX, Yan DS (2007) Mater Sci Eng A 454–455:132
11. Tian WB, Vanmmeensel K, Wang PL, Zhang GJ, Li YX, Vleugels J, Van der Biest O (2007) Mater Lett 61:4442
12. Lin ZJ, Li MS, Wang JY, Zhou YC (2007) Acta Mater 55:6182
13. Lee DB, Nguyen TD, Han JH, Park SW (2007) Corros Sci 49:3926
14. Barsoum MW, El-Raghy T, Ogbuji LUJT (1997) J Electrochem Soc 144:2508
15. Wang XH, Zhou YC (2003) Corros Sci 45:891
16. Yang SL, Sun ZM, Hashimoto H, Park YH, Abe T (2003) Oxidat Metal 59:155
17. Sun ZM, Zhou YC, Li MS (2001) Corros Sci 43:1095
18. Lee DB, Park SW (2006) Mater Sci Eng A 434:147
19. Dean JA (1999) Lange's handbook of chemistry, 15th edn. McGraw-Hill Book Co, New York, p 6.82
20. Dean JA (1999) Lange's handbook of chemistry, 15th edn. McGraw-Hill Book Co, New York, p 6.90
21. Zhang HB, Zhou YC, Bao YW, Li MS (2004) Acta Mater 52:3631